Dynamic response of a Fabry–Perot interferometer

M. J. Lawrence, B. Willke, M. E. Husman, E. K. Gustafson, and R. L. Byer

Ginzton Laboratory, Stanford University, Stanford, California 94305

Received July 9, 1998; revised manuscript received November 16, 1998

We predict and measure the temporal response of a Fabry–Perot cavity field to changes in cavity length and frequency of the incident laser field. We outline the theoretical differences between changes in the cavity-length and laser-frequency modulation and present a theoretical derivation of the time response of the resulting cavity field and its effect on the reflected field, the transmitted field, and the Pound–Drever–Hall error signal. We show that oscillations in the resulting signals are due to oscillations in the amplitude and the phase of the cavity field itself. Finally, we demonstrate how induced cavity-field oscillations may be used to determine the mirror velocity or the frequency change of the injected laser field. © 1999 Optical Society of America [S0740-3224(99)00404-X]

OCIS codes: 140.4780, 120.2230, 120.3180.

1. INTRODUCTION

Since its introduction in 1899,[1] the Fabry–Perot interferometer has been used extensively in spectroscopy, interferometry, and maser and laser resonators.[2] Until recently, however, the use of the Fabry–Perot in the optical regime has been limited to the observation of the cavity's static response. Advances in lasers and optical coatings now offer the opportunity to explore the time response of the Fabry–Perot interferometer. It is of interest to note, however, that this dynamic behavior has been previously observed in a high-Q superconducting cavity with a swept microwave source.[3]

In this paper we present a theory of the dynamic response of the Fabry–Perot's cavity field. Self-consistent field equations are used to develop a series expansion for changes in both the cavity length and the laser frequency. These series expansions are then reduced to differential equations that are easily solved and offer insight into the dynamics of the cavity field. We present the time response of a Fabry–Perot's reflected and transmitted fields. We also examine the time response of the Pound–Drever–Hall error signal. We obtain excellent agreement between theory and experiment.

Both theory and experiment show that temporal oscillations occur in the measured signals and that these oscillations are due, in part, to modulation of the field inside the cavity and not solely due to a beating between the cavity field and the directly reflected signal as previously supposed.[4] The oscillations are observable when the cavity length or the input frequency is modulated within a cavity storage time by half of a full-width half-maximum (fwhm) at cavity-resonance peak width.

Precision interferometry, such as the laser interferometric detection of gravitational waves,[5] and precision spectroscopy, such as cavity-locked ring-down spectroscopy,[6] drive the need to understand the temporal response of Fabry–Perot interferometers. Understanding and predicting the temporal response of Fabry–Perot cavities is of intrinsic interest but is also important for automated cavity-length and alignment-control systems.[7–10]

For example, for the 4-km-long Laser Interferometer Gravitational-Wave Observatory (LIGO) Fabry–Perot interferometer with a finesse of 200 and a fwhm cavity linewidth of 150 Hz, a mirror velocity of 5.2 μm/s, or a laser-frequency sweep speed of 375 kHz/s, is sufficient to yield oscillations. Finally, we show how the oscillating reflected field may be used to determine the rate of incident-frequency change or cavity-length change, and how the oscillating Pound–Drever–Hall signal may degrade the Pound–Drever–Hall frequency-stabilization method.[11]

2. TIME RESPONSE OF A FABRY–PEROT INTERFEROMETER

A. Static Cavity

Consider a field incident on a Fabry–Perot[12] cavity, as shown in Fig. 1. The cavity is defined by two mirrors a distance L apart and is resonant with the laser when the field acquires a $2m\pi$ phase shift in a cavity round trip, where m is an integer. When this resonance condition is met, the light that enters through the input mirror constructively interferes with light that entered at earlier times, resulting in a significant cavity field.

Here we make use of the phasor representation of fields to graphically represent the components of the cavity field. To introduce this representation, as well as to provide a comparison for what occurs when the cavity length or the field frequency is modulated, first we describe the steady-state behavior of the cavity field in terms of the phasor picture.

In the phasor representation, the time-oscillating components of fields are removed by choosing a reference frame that rotates in time at the field frequency. For example, the phasor representation of the field $\tilde{E}_1 = E_1 \exp[i(k_1 x - \omega_1 t)]$, obtained by multiplication by $\exp(i\omega_1 t)$, is $E_1 \exp(ik_1 x)$. The phasor is a vector whose magnitude is equal to the magnitude of $E_1 \exp(ik_1 x)$ and

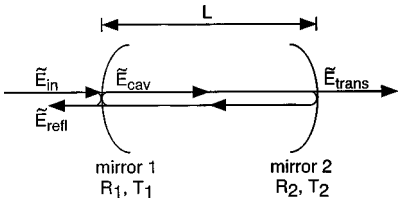

Fig. 1. Laser light entering a Fabry–Perot cavity. The input field, $\tilde{E}_{\mathrm{in}}$, results in a cavity field, $\tilde{E}_{\mathrm{cav}}$. Transmission of the cavity field yields the transmitted field, $\tilde{E}_{\mathrm{trans}}$, while interference between the directly reflected input field and the transmitted cavity field produces the reflected field, $\tilde{E}_{\mathrm{refl}}$.

whose angle indicates the phase of $E_1 \exp(ik_1x)$ relative to its phase at a particular value of x. While the field itself oscillates as a function of both position and time, the phasor oscillates only as a function of position. For a field oscillating at a different frequency, $\tilde{E}_2 = E_2 \exp[i(k_2x - \omega_2t)]$, the phasor representation in the same reference frame is $E_2 \exp\{i[k_2x - (\omega_2 - \omega_1)t]\}$. Its phasor rotates as both the time and the distance change.

Figure 2 shows the phasor representation of the components and resulting cavity field for the near-resonant and off-resonant conditions. Phasors that are in phase with the incident field are plotted along the horizontal axis, while phasors that are shifted by $\pi/2$ are plotted along the vertical axis. The individual components represent the field transmitted into the cavity each round trip. Near resonance, the phasors acquire only a small phase shift in a round trip, and the nearly parallel phasors combine to yield a large cavity field.

The field transmitted through the cavity depends solely on the amplitude of the cavity field and is therefore a maximum at the resonant condition. The field reflected from the Fabry–Perot cavity is the superposition of the directly reflected input field and the cavity field that passes back through the input mirror. The $\pi/2$ phase shift that the incident field acquires upon entering the leaving the cavity leads to destructive interference with the directly reflected field. As a result, the reflected power is a minimum when the cavity resonant frequency equals the frequency of the input beam.

If the cavity is not resonant, the components of the cavity field acquire a wide range of phase shifts after circulating within the cavity and tend to destructively interfere and produce a negligible cavity field. This smaller field results in a reduced amplitude for the transmitted field and an increased amplitude for the field reflected from the cavity compared with the resonant condition.

This steady-state behavior of the reflected and the transmitted fields as a function of the input laser frequency is well known.[13] In transmission, the cavity acts as a narrowband transmission filter. The fwhm cavity linewidth is the distance in frequency between the two points on either side of the maximum transmission where the intensity falls to half of its maximum value.[14] In units of radians per second, it is given by

$$\Delta\omega_{\mathrm{fwhm}} = \frac{\pi c}{L\mathcal{F}}, \tag{1}$$

where c is the speed of light, $\pi c/L$ is the cavity free spectral range in radians per second, and $\mathcal{F}$ is the cavity finesse. For low loss, it has been shown[15] that the finesse can be written as

$$\mathcal{F} = \frac{\pi(R_1R_2)^{1/4}}{1 - \sqrt{R_1R_2}},$$

where R_1 and R_2 are the power-reflection coefficients of the two mirrors.

Higher reflectivities, or higher finesses, result in phasors that remain within the cavity for a longer time. In a high-finesse cavity, phasors can still be of a significant amplitude when, after numerous round trips, they have acquired enough phase to destructively interfere with the other phasors in the cavity. The result is a narrower linewidth. Input fields whose frequencies are several linewidths from the resonance condition can be considered to be directly reflected, and the resulting cavity field is small.

If the length of the cavity changes, instead of the input laser frequency, we may use an alternative expression for the fwhm cavity linewidth. Moving the end mirror by a distance $\lambda/2$ is equivalent to moving the input laser frequency by the free spectral range. Thus the distance in cavity length between the two points on either side of the maximum transmission where the intensity falls to half of its maximum value is given by

$$\Delta L_{\mathrm{fwhm}} = \frac{\lambda/2}{\mathcal{F}} = \frac{\pi c}{\omega\mathcal{F}}. \tag{2}$$

If we phase modulate the input field at frequency ω_m with small modulation depth δ, the resulting field can be described to first order by a central carrier field with two sidebands[16] given by

$$\tilde{E}_{\mathrm{in}} = E_0\Big(\exp(-i\omega t) + \frac{\delta}{2}\{\exp[-i(\omega + \omega_m)t] - \exp[-i(\omega - \omega_m)t]\}\Big). \tag{3}$$

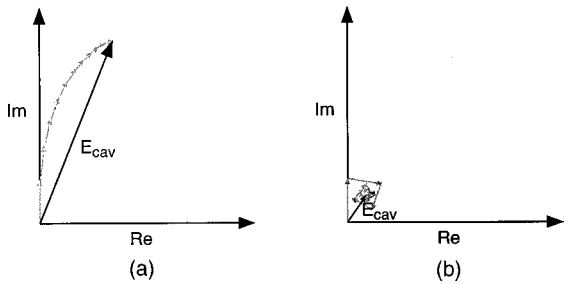

Fig. 2. Phasor representation of the cavity field near the resonant condition and at the off-resonant condition. The phasor components are shown in gray and the cavity field in black. The horizontal axis represents signals in phase with the input field, and the vertical axis represents signals $\pi/2$ out of phase with the input field. Near the resonant condition, all phasors acquire a phase shift close to an integer multiple of 2π after each round trip, and they constructively interfere to produce a large cavity field. At the off-resonant condition, all phasors acquire a phase shift significantly different from an integer multiple of 2π after each round trip, and they destructively interfere to produce a small cavity field.

If the carrier frequency, ω, is close to a resonant frequency defined by the cavity and the modulation frequency, ω_m, is significantly larger than several cavity linewidths, the sidebands are directly reflected while some of the unmodulated carrier builds up to a cavity field, $\tilde{E}_{\mathrm{cav}}$, inside the Fabry–Perot. This cavity field, defined just inside the input mirror, has the same frequency as the incident carrier light: $\tilde{E}_{\mathrm{cav}} = E_{\mathrm{cav}} \exp[i(kx - \omega t)]$. The transmitted field is given by

$$\tilde{E}_{\mathrm{trans}} = i\sqrt{T_2}\tilde{E}_{\mathrm{cav}}.$$

The time-averaged transmitted optical intensity is therefore

$$I_{\mathrm{trans}} = \frac{1}{2} c \epsilon_0 \tilde{E}_{\mathrm{trans}} \tilde{E}^*_{\mathrm{trans}} = \frac{1}{2} c \epsilon_0 T_2 E_{\mathrm{cav}} E^*_{\mathrm{cav}},$$

where c is the speed of light, ϵ_0 is the permittivity of free space, and T_2 is the power-transmission coefficient of the output mirror. If the light beam is smaller than the photodetector area, the resulting current is

$$i_{\mathrm{trans}} = \mathcal{R} I_{\mathrm{trans}} = \frac{1}{2} c \epsilon_0 \mathcal{R} T_2 E_{\mathrm{cav}} E^*_{\mathrm{cav}}, \tag{4}$$

where $\mathcal{R}$ is the responsivity of the detector in amperes per watt.

The field reflected from the cavity consists of the directly reflected input beam combined with a component of the cavity field transmitted out of the cavity through the input mirror and is given by

$$\tilde{E}_{\mathrm{refl}} = \sqrt{R_1}\tilde{E}_{\mathrm{in}} \exp\left(\frac{-i2\omega L}{c}\right) + i\sqrt{T_1 R_2}\tilde{E}_{\mathrm{cav}},$$

where T_1 is the power-transmission coefficient of the input mirror. For a cavity near resonance, $\exp(-i2\omega L/c) \approx 1$, and the reflected field can be written as

$$\begin{aligned}\tilde{E}_{\mathrm{refl}} = {} & \sqrt{R_1} E_0 \exp(-i\omega t) \\ & \times \left\{1 + \frac{\delta}{2}[\exp(-i\omega_m t) - \exp(i\omega_m t)]\right\} \\ & + i\sqrt{T_1 R_2} E_{\mathrm{cav}} \exp(-i\omega t)\end{aligned} \tag{5}$$

with the corresponding time-averaged optical intensity

$$I_{\mathrm{refl}} = \frac{1}{2} c \epsilon_0 \tilde{E}_{\mathrm{refl}} \tilde{E}^*_{\mathrm{refl}}.$$

Detection of this reflected field with a photodetector yields the time-averaged current

$$i_{\mathrm{refl}} = \mathcal{R} I_{\mathrm{refl}} = \frac{1}{2} c \epsilon_0 \mathcal{R} \tilde{E}_{\mathrm{refl}} \tilde{E}^*_{\mathrm{refl}}. \tag{6}$$

For the static case, the reflected current will have a dc term, a term at frequency ω_m, and a term at frequency $2\omega_m$. All these terms can be found by substitution of the expression for the reflected field, Eq. (5), into the expression for the reflected current, Eq. (6). Direct measurement of the reflected current is dominated by the dc term

$$\begin{aligned}i_{\mathrm{refl}} = {} & \frac{1}{2} c \epsilon_0 \mathcal{R} [R_1 E_0^2 - 2\sqrt{T_1 R_1 R_2} E_0 \operatorname{Im}(E_{\mathrm{cav}}) \\ & + T_1 R_2 E_{\mathrm{cav}} E^*_{\mathrm{cav}}].\end{aligned} \tag{7}$$

The component of the reflected current at the modulation frequency ω_m is the Pound–Drever–Hall signal,[11]

$$i_{\mathrm{pdh}} = -c \epsilon_0 \mathcal{R} \sqrt{T_1 R_1 R_2}\, \delta E_0 \operatorname{Re}(E_{\mathrm{cav}}). \tag{8}$$

We therefore have three signals at our disposal that offer information about the cavity field: i_{trans}, i_{refl}, and i_{pdh}. The first is proportional to the amplitude of the cavity field. The second contains information about both the amplitude of the cavity field and its phase relative to the input field. The third measures the phase of the cavity field relative to the input field. We next investigate the dynamic behavior of the cavity field as the cavity length or the input field's frequency is modulated.

B. Cavity-Length Modulation

Consider a light beam of frequency ω and amplitude E_0 incident upon a Fabry–Perot cavity. Now, however, the distance between the cavity mirrors is a function of time, given by L_t. If the cavity initially is empty, the only component of the cavity field immediately after the beam is turned on is that transmitted through the input mirror. As a result, the cavity field is given by

$$\tilde{E}_{\mathrm{cav}} = i\sqrt{T_1} E_0 \exp[i(kx - \omega t)].$$

At the end mirror, the field's frequency is changed owing to the Doppler shift resulting from the reflection from a moving mirror. The component's amplitude is reduced because of transmission at each mirror and loss in the cavity. At the input mirror, it is combined with additional transmitted input light whose phase is determined by the time it took the first component to complete its trip. The cavity field is now given by

$$\begin{aligned}\tilde{E}_{\mathrm{cav}} = i\sqrt{T_1} E_0 \Bigg(& \exp(-i\omega\tau) \exp\{i[kx - \omega(t - \tau)]\} \\ & + \rho \exp\left\{ i\left(1 + \frac{2\dot{L}_{\tau/2}}{c}\right)[kx - \omega(t - \tau)]\right\}\Bigg),\end{aligned}$$

where τ is the unperturbed round-trip time, given by

$$\tau = \frac{2L}{c},$$

and ρ is the round-trip loss factor, $\sqrt{R_1 R_2}\exp(-2\alpha L)$, α being the field loss in the cavity. Here $k(1 + 2\dot{L}_{\tau/2}/c)$ and $\omega(1 + 2\dot{L}_{\tau/2}/c)$ are the wave vector and the frequency after reflection from a mirror with velocity $\dot{L}_{\tau/2}$, where we assume that the end mirror is moving toward the input mirror.

This discrete sum of fields can then be extended to an integer number, n, of round trips later in time:

$$\tilde{E}_{\mathrm{cav}} = i\sqrt{T_1}E_0\Bigg(\exp(-i\omega n\tau)\exp\{i[kx - \omega(t - n\tau)]\} + \rho\exp[-i\omega(n-1)\tau]\exp\left\{i\left(1 + \frac{2\dot{L}_{(2n-1)\tau/2}}{c}\right)\times[kx - \omega(t - n\tau)]\right\} + \rho^2\exp[-i\omega(n-2)\tau]\exp\left\{i\left(1 + \frac{2\dot{L}_{(2n-1)\tau/2}}{c}\right)\times\left(1 + \frac{2\dot{L}_{(2n-3)\tau/2}}{c}\right)[kx - \omega(t - n\tau)]\right\} + \ldots + \rho^n\exp\left\{i\left(1 + \frac{2\dot{L}_{(2n-1)\tau/2}}{c}\right)\times\left(1 + \frac{2\dot{L}_{(2n-3)\tau/2}}{c}\right)\cdots\left(1 + \frac{2\dot{L}_{\tau/2}}{c}\right)\times[kx - \omega(t - n\tau)]\right\}\Bigg). \quad (9)$$

The resulting cavity field is a superposition of fields that entered the cavity at times separated by the round-trip time. If the length of the cavity remains fixed, the cavity field reaches a steady-state value. If, however, the cavity changes length such that the terms in Eq. (9) acquire significantly different phases relative to the static case before they become insignificant in size, the cavity field may be modulated in both phase and amplitude.

Figure 3 shows the phasor representation of the cavity fields at times $n\tau$ and $(n + 1)\tau$. The cavity field at any time is the vector sum of the phasors. In the phasor picture, the input field remains fixed in phase, and the cavity-field components rotate as they travel around the cavity. After a round trip, a phasor is reduced in amplitude owing to loss and rotated because of the acquired phase shift. Although the phasors present in the cavity at any time represent fields of different frequencies (as different phasors have experienced a different number of Doppler shifts), they all acquire the same phase shift and the same loss in one round trip. Therefore at any time

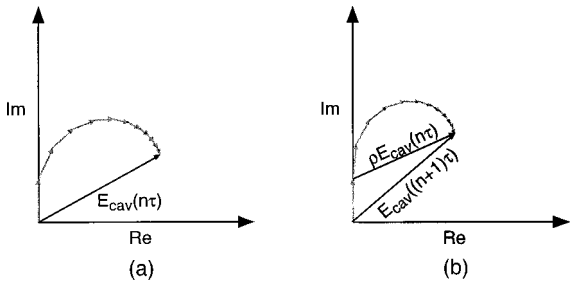

Fig. 3. Cavity field at times $n\tau$ and $(n + 1)\tau$ with a moving end mirror. Since all phasors acquire the same loss and phase shift within a round trip, they can be replaced by their sum phasor. Instead of keeping track of the individual phasors, this sum phasor can then be reduced (multiplied by ρ), rotated by the round-trip phase, and then added to the transmitted input beam to yield the cavity field a round trip later in time.

we can replace the individual phasors with their resultant phasor, the cavity field, and simply propagate it around the cavity and combine it with the next transmitted incident beam to determine the cavity field a round trip later.

As the phasor picture suggests, there is a recursion relationship that relates the cavity field to both the input field and the cavity field that existed a round-trip time before[15]:

$$E_{\mathrm{cav}}(t + \tau) = i\sqrt{T_1}E_0 + \rho\exp\left(\frac{i2\omega L_{t+\tau/2}}{c}\right)E_{\mathrm{cav}}(t).$$

For small offsets from the resonance condition, the effect of the phase shift acquired by the field after one trip, $\exp(i2\omega L_{t+\tau/2}/c)$, is approximately $1 + i(2\omega\dot{L}t/c)$, where $\dot{L}t$ is the time-varying offset from resonance. If neither the cavity nor the input beam change significantly within a round trip, the recursion relation can be rewritten as a linear differential equation:

$$\frac{\mathrm{d}E_{\mathrm{cav}}}{\mathrm{d}t} = \left(\frac{\rho - 1}{\tau} + \frac{i2\rho\omega\dot{L}}{\tau c}t\right)E_{\mathrm{cav}} + \frac{i\sqrt{T_1}}{\tau}E_0. \quad (10)$$

Care is required when transforming from the discrete time step of a round trip to a continuous time variable. The recursion relation accurately describes the cavity field after a round trip, including Doppler effects. However, it does not account for the different phases acquired by the individual components over smaller time intervals. The resulting error will be small if the additional phase acquired by each component over a round trip is small.

The cavity storage time, τ_s, is the time required for a $1/e$ decay of the cavity field. This can be determined by application of Eq. (10) to a fixed cavity before and after the input is turned off. By use of the fact that $\rho \approx (1 - \pi/\mathcal{F})$ for high finesses, the resulting storage time is given by

$$\tau_s \approx \frac{\mathcal{F}\tau}{\pi} = \frac{2\mathcal{F}L}{\pi c}.$$

We can normalize the time scale of the cavity field in Eq. (10) with respect to the cavity storage time by defining the new variable $t' = t/\tau_s$. As a result, Eq. (10) becomes

$$\frac{\mathrm{d}E_{\mathrm{cav}}}{\mathrm{d}t'} = -(1 - i\nu_L t')E_{\mathrm{cav}} + i\frac{\sqrt{T_1}\mathcal{F}}{\pi}E_0, \quad (11)$$

where the ν_L, the normalized length scan rate, is given by

$$\nu_L = \frac{2\mathcal{F}\omega\dot{L}\tau_s}{\pi c}. \quad (12)$$

From Eq. (2) we can see that ν_L is simply the number of half fwhm cavity linewidths moved by the mirror within a cavity storage time or

$$\nu_L = \frac{\dot{L}}{(\Delta L_{\mathrm{fwhm}}/2)/\tau_s}. \quad (13)$$

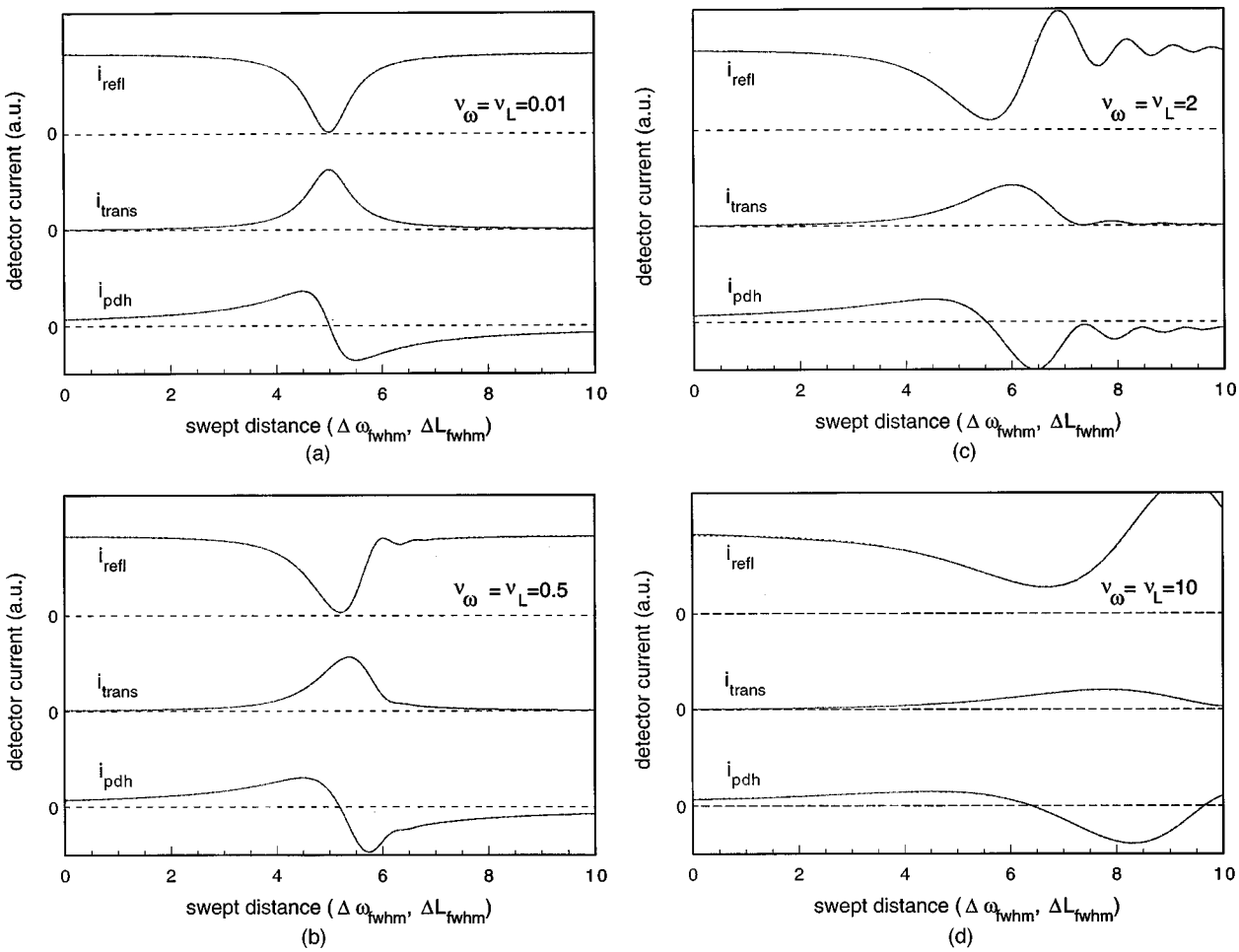

Fig. 4. Theoretical transmitted, reflected, and Pound–Drever–Hall error photodetector signals for $\nu_L = \nu_\omega$ equal to (a) 0.01, (b) 0.5, (c) 2, and (d) 10 from Eqs. (11) and (16). The horizontal axes represent the distance sweep in units of fwhm cavity linewidths: $\Delta\omega_{\text{fwhm}}$ for frequency sweeps, and ΔL_{fwhm} for length sweeps. This distance is given by half the normalized time, $t/2\tau_s$, multiplied by ν_ω or ν_L. Oscillations are visible when ν_ω or ν_L approach 1. The curves are offset in the vertical direction for clarity. Also plotted for all figures are the series expressions, Eqs. (9) and (14). The curves are indistinguishable from the differential equation solutions.

C. Frequency Modulation of the Input Field

Consider next an input beam whose frequency varies with time instead of a moving cavity mirror. As for the length-modulation case, we can derive a series expression for the cavity beam. Initially, the only field inside the cavity is that transmitted through the input mirror. The cavity field, defined just beyond the input mirror, is given by

$$\tilde{E}_{\text{cav}} = i\sqrt{T_1}E_0 \exp[i(k_0 x - \omega_0 t)],$$

where ω_0 and k_0 are the wave vector and the frequency at $t = 0$.

After one round trip, this cavity field is reduced in amplitude. At the input mirror, the cavity field interferes with some transmitted input field, now at frequency ω_τ, and becomes

$$\tilde{E}_{\text{cav}} = i\sqrt{T_1}E_0(\exp(-i\omega_\tau\tau)\exp\{i[k_\tau x - i\omega_\tau(t - \tau)]\} + \rho \exp\{i[kx - \omega_0(t - \tau)]\}).$$

An integer number, n, of round trips later in time,

$$\begin{aligned}\tilde{E}_{\text{cav}} = i\sqrt{T_1}E_0\{&\exp(-i\omega_{n\tau}n\tau)\exp[ik_{n\tau}x - \omega_{n\tau}(t - n\tau)] \\ &+ \rho \exp[-i\omega_{(n-1)\tau}(n - 1)\tau]\exp[ik_{(n-1)\tau}x \\ &- \omega_{(n-1)\tau}(t - n\tau)] \\ &+ \rho^2 \exp[-i\omega_{(n-2)\tau}(n - 2)\tau]\exp[ik_{(n-2)\tau}x \\ &- \omega_{(n-2)\tau}(t - n\tau)] + \cdots \\ &+ \rho^n \exp[ik_0 x - \omega_0(t - n\tau)]\}. \end{aligned} \quad (14)$$

This expression is similar to the series expression for the length-modulation case, Eq. (9), and can be recast as the differential equation

$$\frac{dE_{\text{cav}}}{dt} = \left(\frac{\rho - 1}{\tau} + \frac{i2\rho\dot{\omega}L}{\tau c}t\right)E_{\text{cav}} + \frac{i\sqrt{T_1}}{\tau}E_0. \quad (15)$$

Normalization of the rate of change of the cavity field with respect to the cavity lifetime results in

$$\frac{dE_{\text{cav}}}{dt'} = -(1 - i\nu_\omega t')E_{\text{cav}} + i\frac{\sqrt{T_1}\mathcal{F}}{\pi}E_0, \quad (16)$$

where $t' = t/\tau_s$ and the normalized frequency scan rate, ν_ω, is given by

$$\nu_\omega = \frac{2\mathcal{F}L\dot{\omega}\tau_s}{\pi c}. \tag{17}$$

From Eq. (1) we can see that ν_ω is simply the number of half fwhm cavity linewidths swept by the input laser frequency within a cavity storage time, or

$$\nu_\omega = \frac{\dot{\omega}}{(\Delta\omega_{\text{fwhm}}/2)/\tau_s}. \tag{18}$$

The differential equations that give the cavity field in the case of length and frequency modulation, Eqs. (11) and (16), are equivalent if one considers the time derivative of the product ωL.

3. THEORETICAL RESULTS

From Eqs. (11) and (16) it is apparent that E_{cav} has an oscillating component when ν_L or ν_ω are nonzero. Whether the oscillations are apparent or not depends on their size. For $\nu_L \ll 1$ or $\nu_\omega \ll 1$, corresponding to sweeps less than half of a fwhm cavity linewidth per storage time, the oscillations will not be observed. However, when the normalized scan rates are comparable to 1, the oscillations in the cavity field will be significant and result in oscillations in the three measured photodetector currents.

Theoretical plots of i_{trans}, i_{refl}, and i_{pdh} derived from Eqs. (11) and (16) for $\nu_L = \nu_\omega$ equal to 0.01, 0.5, 2, and 10 are shown in Figs. 4(a)–4(d). The horizontal axes of the plots represent the distance swept by the cavity mirror or laser frequency in units of fwhm cavity linewidths: $\Delta\omega_{\text{fwhm}}$ for frequency sweeps and ΔL_{fwhm} for length sweeps. This normalized distance is simply half the normalized time, $t/2\tau_s$, multiplied by ν_ω or ν_L. As expected, oscillations are visible when ν_ω and ν_L are close to 1. Also plotted are the results from the series equations themselves, Eqs. (9) and (14). The curves resulting from the differential equations are indistinguishable from those resulting from the series equations.

Our experimental observations confirm the cavity-field behavior predicted by our theory.

4. EXPERIMENT

A. Setup

The experimental setup used to measure the Fabry–Perot time response to both frequency and length modulation is shown in Fig. 5. The Fabry–Perot ring cavity had a perimeter of 42 cm and a finesse of 4000 for *S*-polarized light and 220 for *P*-polarized light. Its end mirror was mounted on a piezoelectric transducer (PZT) to enable us to sweep the cavity and measure the cavity-field dependence on length change. The laser was a single-axial-mode 300-mW Lightwave Model 122 with both fast (PZT) and slow (thermal) frequency actuators. The measurement of oscillations in the transmitted field, the reflected field, and the Pound–Drever–Hall signal required a high-finesse cavity with length control and a laser with frequency control.

The two polarizations were resonant with the ring cavity at different frequencies and with different finesses. This enabled us to separate the *S*- and *P*-polarized light, using one polarization to lock the cavity to the laser while the other one was swept in frequency. This ensured that changes in the cavity length did not affect our frequency-modulation results. The *P* polarization was used to lock the laser frequency to the cavity by use of the Pound–Drever–Hall method, and the *S* polarization was used to determine the cavity-field dependence upon length and frequency changes. After the polarizations had been spatially separated with a polarizing beam splitter (PBS), the *P*-polarized light was phase modulated with an electro-optic modulator (EOM1) and introduced into the cavity. The *P*-polarized component of the light reflected from the cavity was measured by a photodetector. The resulting signal was demodulated and sent to a control circuit with two outputs: a fast control signal sent to the PZT input

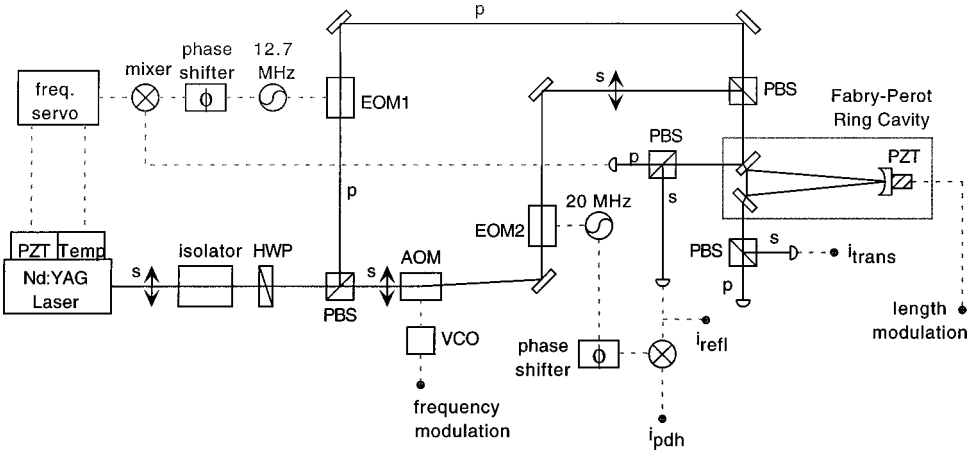

Fig. 5. Experimental apparatus used to measure the time response of the Fabry–Perot cavity for both the length- and the frequency-modulation schemes. The cavity had a round-trip length of 42 cm and a finesse of 4000 for *S*-polarized light and a finesse of 220 for *P*-polarized light. The *P*-polarized laser beam was used to lock the laser frequency to the cavity with the traditional Pound–Drever–Hall method. An acousto-optic modulator was used to change the frequency of the *S*-polarized light. For length modulation the *S*-polarized beam was unused and a piezoelectric actuator was used to change the cavity length.

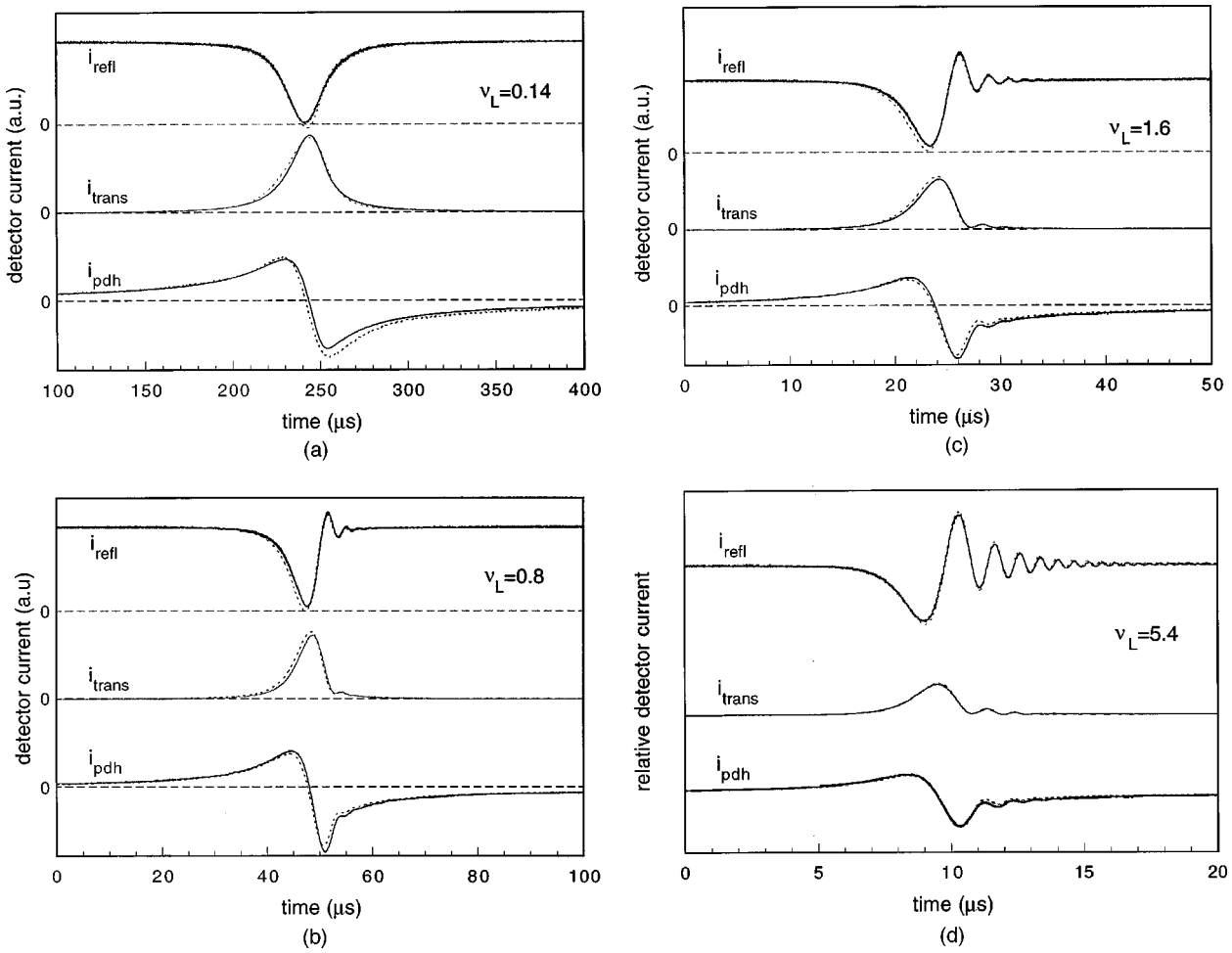

Fig. 6. Time response of the Fabry–Perot cavity's reflected, transmitted, and Pound–Drever–Hall error photodetector currents for mirror velocities ν_L equal to (a) 0.14, (b) 0.8, (c) 1.6, and (d) 5.4 as a function of sweep time. The curves have been offset in the vertical direction for clarity, and the dashed lines indicate zero current. The dotted lines indicate the theoretical fits to the experimental results. The storage time of the cavity was 1.8 μs. The theoretical fits are in excellent agreement with the measured data, and, as predicted, oscillations are observed when the normalized sweep speed is of the order of 1.

of the laser, and a slow control signal sent to the thermal input of the laser.

The *S*-polarized light was shifted in frequency with an acousto-optic modulator (AOM). The signal sent to the modulator consisted of a dc and an rf component. The dc component was required to shift the frequency of the *S*-polarized light so that it was resonant at the same cavity length as the *P*-polarized light. The rf component was used to modulate the frequency of the *S*-polarized light. These two signals were combined with a bias-Tee, a passive electronic circuit specifically designed to combine dc and rf signals, and the resulting signal was sent to a voltage-controlled oscillator (VCO). Output from the oscillator was then fed to the acousto-optic modulator. To accurately center the *S* polarization on resonance, a Keithley 263 Calibrator/Source was used to provide the dc signal. After the frequency modulation, the *S*-polarized light was phase modulated with EOM2 and then recombined with the *P*-polarized light with a polarizing beam splitter before being sent into the cavity. Before detection, the *S*-polarized reflected and transmitted beams were separated from the *P*-polarized beams. The unde-modulated reflected signal was retrieved directly with the photodetector measuring the *S*-polarized reflected light.

The Pound–Drever–Hall signal is proportional to the component of the reflected field oscillating at the phase-modulation frequency. This signal was obtained by electronic demodulation of the reflected signal with the local oscillator driving the phase modulator. An rf phase shifter was used to compensate for delay times between these two signals. The resulting signal was then passed through a low-pass filter to remove higher-frequency components.

For length-modulation experiments the laser frequency could not be locked to the cavity length; otherwise, length modulation would result in laser-frequency modulation. We blocked the *S*-polarized light passing through the acousto-optic modulator and used a half-wave plate to rotate the polarization of the light in the former *P*-polarized path to *S* polarization. The cavity length was changed by application of a high-voltage triangular signal to the cavity PZT. Drift in the laser frequency had a negligible effect on the cavity field compared with the effect of the large relative changes in length. As for the frequency-

modulation case, we measured the transmitted and the reflected light, and we demodulated the reflected light signal to obtain the Pound–Drever–Hall signal.

B. Measurements

Using the apparatus in Fig. 5, we measured the reflected and the transmitted photodetector currents and the Pound–Drever–Hall signals. We then fitted our differential equations, Eqs. (10) and (15), to our measurements. The cavity finesse was determined by the value that produced the closest agreement with all of the experimental data acquired with the cavity. Because of different responsivities and electrical offsets of the photodetectors, we determined a scaling factor and offset for each signal, which we then kept constant for all length and frequency scans. Once these values had been set, the only free parameter remaining for fitting theory to each experimental result was the mirror velocity or the frequency sweep speed.

C. Discussion

The measured reflected and transmitted photodetector currents and the Pound–Drever–Hall signals are shown in Fig. 6 for the length scan and in Fig. 7 for the frequency scan. In all plots the three signals are offset in the vertical scale for clarity and the dashed lines indicate zero current. The top curve is the reflected signal, the middle curve is the transmitted signal, and the bottom curve is the Pound–Drever–Hall signal. The fitted theoretical results, calculated from differential equations, Eqs. (10) and (15), are shown on the same figures as dotted lines.

For the length-modulation results shown in Fig. 6(a) the reflected and the transmitted signals show the well-known steady-state Fabry–Perot responses[13]: a decrease in the reflected power as the cavity reaches the resonance condition, along with a corresponding increase in the transmitted power. At this mirror speed the cavity field has enough time to reach a steady-state value before the cavity changes to a new length. In this static regime the Pound–Drever–Hall error signal is an ideal error signal for controlling the cavity length or the laser frequency so that they are resonant with each other. Near resonance, the signal is linear, and it passes through zero when the resonant condition is met. Such an error signal can be used in a simple feedback control system to maintain resonance between the laser and the cavity.[17,18]

Fitting theory to our data, shown in Fig. 6(a), yielded a mirror velocity of 5.8 μm/s, which is equivalent to $\nu_L = 0.14$. This velocity agrees well with the value calculated from the signal sent to the cavity's PZT.

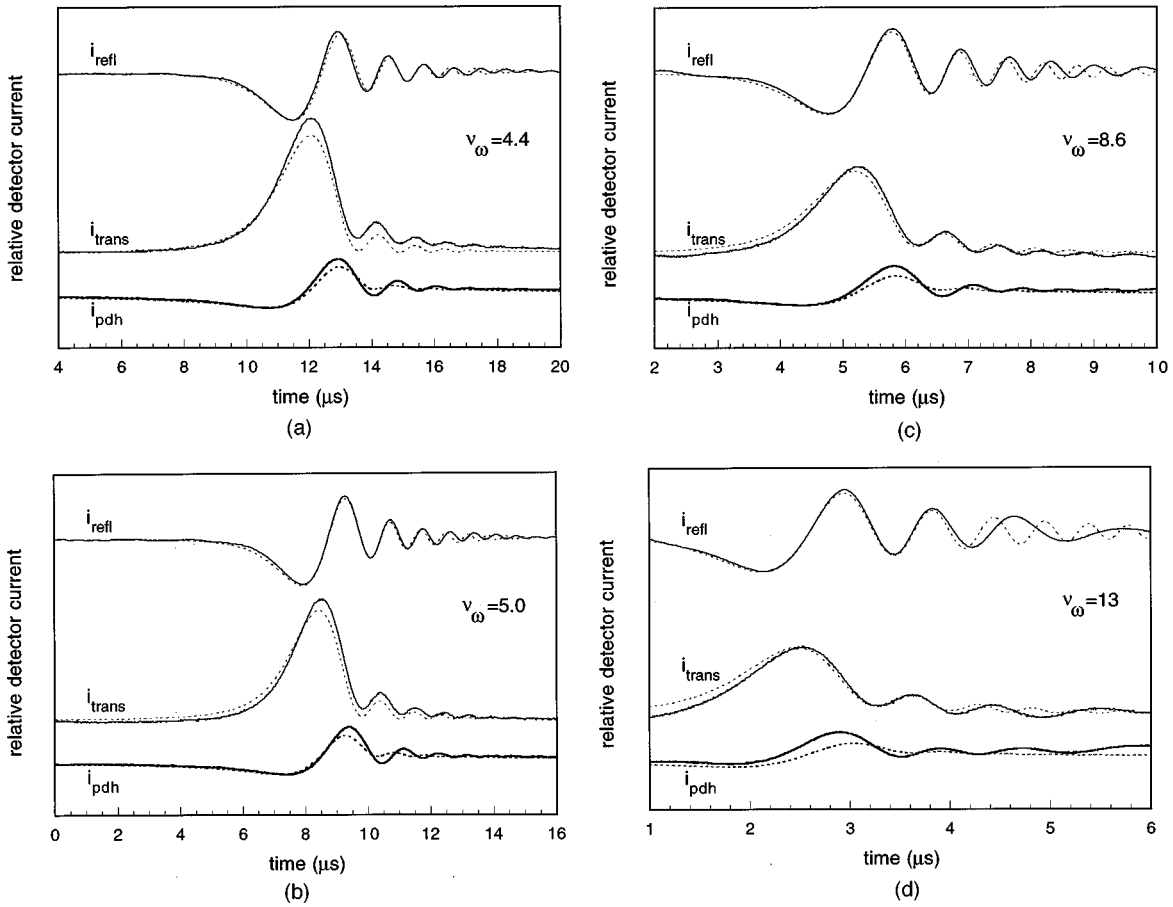

Fig. 7. Time response of the Fabry–Perot cavity's reflected, transmitted, and Pound–Drever–Hall error photodetector currents for frequency sweep speeds ν_ω equal to (a) 4.4, (b) 5.0, (c) 8.6, and (d) 13 as a function of sweep time. The curves have been offset in the vertical direction for clarity, and the dashed lines indicate zero current. The dotted lines indicate the theoretical fits to the experimental results. The storage time of the cavity was 1.8 μs. The theoretical fits are in good agreement with the measured data, although they diverge at longer times owing to the nonlinear frequency sweep produced by our experiment.

The signals resulting from three successively faster mirror velocities are shown in Figs. 6(b)–6(d). At these higher mirror velocities, oscillations arise in all three of the signals. As the velocity increases, the oscillations become more pronounced and increase in frequency. Theoretical fits to the curves, with mirror velocity as the only free parameter, are also shown in dotted lines. The fitted velocities were 30, 50, and 200 μm/s, which correspond to ν_L equal to 0.8, 1.6, and 5.4, respectively.

As the signals are dependent upon both mirror speed and cavity loss, they can be used to determine these parameters. In particular, the reflected signal is ideal for determining their values. Its larger and more numerous oscillations are due to the directly reflected field, which acts as a local oscillator field at the photodetector, as can be seen from Eq. (7).

The transmitted signals clearly show that the oscillations observed in the reflected signal are the effect of the modulated cavity field and are not due to the beating between a frequency-shifted cavity field and the directly reflected field. These signals are produced by the detection of the field that is transmitted through the cavity. This field is not mixed with the directly reflected beam and, as we have previously shown, is proportional to the cavity field's amplitude. Therefore any oscillation in this signal is due solely to an amplitude oscillation of the cavity field.

The Pound–Drever–Hall error signal is no longer the ideal error signal as a result of the cavity-field modulation: it is neither linear nor zero when passing through the resonance condition. Depending on the mirror velocity and the cavity loss, the oscillations can result in multiple zero crossings. Also, the oscillations can be affected by the electronics used to retrieve the error signal. The low-pass filter, used to pick out the signal at the phase-modulation frequency, may reduce the amplitude of the oscillations. Whether or not these oscillations cause problems in stabilization depends on the actuators used to maintain the resonance condition. High-impedance actuators, such as PZT's, are able to respond quickly to the error signal and reduce any motion before oscillations occur. For gravitational-wave detection, however, the decoupling required between test masses and the environment results in the use of low-impedance actuators, such as magnets and coils, which are incapable of responding quickly enough to prevent the onset of the oscillations.

Frequency modulation yields the signals shown in Figs. 7(a)–7(d). The rapid frequency sweeps result in modulation of the cavity field and the corresponding oscillations in the reflected signal, the transmitted signal, and the Pound–Drever–Hall error signal. As for the length-modulation results, the oscillations increase in frequency and increase in relative size for increasing sweep speed.

The differential equation derived from the recursion relation, Eq. (15), is used to create the dotted fitted curves with the frequency speed sweep as the only free parameter. Fitting theory to the measured signals yielded frequency sweeps of 1.3×10^{12}, 1.6×10^{12}, 2.7×10^{12}, and 4.0×10^{12} rad/s^2. These results correspond to ν_ω equal to 4.4, 5.0, 8.6, and 13. Deviation between measurement and theory at times past the buildup regime can be attributed to a nonlinear frequency sweep. The bias-Tee, used to combine the dc and the ac signals fed to the acousto-optic modulator, had a significant frequency response and reduced the linearity of our triangle sweep.

For the differential equations, Eqs. (10) and (15), to be equivalent to the series expressions, Eqs. (9) and (14), changes in the cavity field must be small during a round-trip time. For length modulation this requires that $\dot{L}\tau \ll \lambda/2$, or $\nu_L \ll 2\mathcal{F}^2/\pi$. For frequency modulation this requires that $\dot{\omega}\tau \ll \pi c/L$, or $\nu_\omega \ll 2\mathcal{F}^2/\pi$. For high-finesse cavities the differential equations agree with the series expressions well into the oscillation regime. It may be of interest to note that the time required to solve the differential equations was over one hundred times less than the time required to solve the series expressions. However, no attempt was made to optimize the computation time of the series solution. Further investigation of the computation times is left for future study.

For the conversion from discrete time steps to a continuous time variable to be accurate, the maximum phase acquired by any component owing to its different frequency must be small throughout a round-trip time. For any component of the cavity field this phase increases with the number of bounces within the cavity. However, after $n_{\max} = \tau_s/\tau$ bounces, a phasor will have decayed to $1/e$ of its initial size. For the length modulation, if the additional phase acquired by this component is to be small, then $2n_{\max}\dot{L}\omega\tau/c \ll 2\pi$, or $\nu_L \ll 2\mathcal{F}$. For the frequency modulation this requires that $n_{\max}\dot{\omega}\tau^2 \ll 2\pi$, or $\nu_\omega \ll 2\mathcal{F}$. The conversion from discrete time steps to continuous time will introduce negligible errors well into the oscillation regime for high-finesse cavities.

For length modulation we expect to see oscillations when $\nu_L \approx 1$ or when $\dot{L} \approx \pi^2 c^2/4L\omega\mathcal{F}^2$, and so we expect this limit to decrease with ω, L, and $\mathcal{F}^2$. In particular, for a LIGO interferometer arm with $L=4$ km, $\lambda=1064$ nm, and $\mathcal{F}=200$, oscillations will be apparent when an end mirror is moving at 5.2 μm/s.

For frequency modulation, oscillations will be measurable when $\nu_\omega \approx 1$ or when $\dot{\omega} = \pi^2 c^2/4L^2\mathcal{F}^2$, and so we expect this limit to decrease with L^2 and $\mathcal{F}^2$. For the same LIGO interferometer arm, oscillations will be apparent when the incident laser frequency has a sweep speed of 375 kHz/s.

For the isolated LIGO test masses and the prestabilized LIGO laser, excursions at these speeds are unlikely. However, for prototype interferometers, which require increased finesses to account for their shorter lengths, oscillating signals may occur. In particular, the mirror motion may be large enough to result in oscillating signals as the mirror velocity threshold decreases with the product $L\mathcal{F}^2$. The frequency sweep speed threshold is less sensitive to this scaling in size as it decreases with the product $L^2\mathcal{F}^2$.

5. CONCLUSIONS

We have fully analyzed the time response of a Fabry–Perot cavity field for the first time. We have obtained excellent agreement between our theory and experimental results. The ability to understand and predict the dynamic behavior of the Fabry–Perot cavity will be of use

for spatial and temporal filtering of lasers, frequency stabilization, interferometer lock acquisition, and ring-down spectroscopy.

Clearly, changes in both cavity length and input laser frequency can induce oscillations in the transmitted and the reflected fields of a Fabry–Perot interferometer and can alter the Pound–Drever–Hall error signal. In particular, oscillations in these signals will be measurable when either ν_L or ν_ω are of the order of 1. Fortunately, a simple linear differential equation can accurately predict the behavior of the cavity field as long as ν_L or ν_ω are much less than $2\mathcal{F}$. While fast changes can make feedback loops, which rely upon the traditional form of the Pound–Drever–Hall error signal, ambiguous, the oscillations can provide useful information of their own. In particular, the reflected signal provides a means of determining the cavity loss and the sweep speed. Knowledge of the sweep speed may be used to reduce the mirror motion and subsequently acquire cavity lock by use of the regular feedback control system, which relies on a valid Pound–Drever–Hall signal.

ACKNOWLEDGMENTS

The authors thank C. Harb for helpful discussions. B. Willke thanks the Alexander von Humboldt-Stiftung for his Feodor-Lynen fellowship. This material is based upon work supported, in whole or in part, by the National Science Foundation under grant PHY-96-30172.

REFERENCES

1. C. Fabry and A. Perot, "Théorie et applications d'une nouvelle méthode de Spectroscopie Interférentielle," Ann. de Chim. et de Phys. **16**, 115 (1899).
2. J. M. Vaughan, *The Fabry-Perot Interferometer: History, Theory, Practice, and Applications* (Hilger, London, 1989).
3. H. J. Schmitt and H. Zimmer, "Fast sweep measurements of relaxation times in superconducting cavities," IEEE Trans. Microwave Theory Tech. **MTT-14**, 206–207 (1966).
4. K. An, C. Yang, R. R. Dasari, and M. S. Feld, "Cavity ring-down technique and its application to the measurement of ultraslow velocities," Opt. Lett. **20**, 1068–1070 (1995).
5. A. Abramovici, W. E. Althouse, R. W. P. Drever, Y. Gürsel, S. Kawamura, F. J. Raab, D. Shoemaker, L. Sievers, R. E. Spero, K. S. Thorne, R. E. Vogt, R. Weiss, S. E. Whitcomb, and M. E. Zucker, "LIGO: the laser interferometer gravitational-wave observatory," Science **256**, 325–333 (1992).
6. B. A. Paldus, C. C. Harb, T. G. Spence, B. Willke, J. Xie, J. S. Harris, and R. N. Zare, "Cavity-locked ring-down spectroscopy," J. Appl. Phys. **83**, 3993 (1998).
7. J. Camp, L. Sievers, R. Bork, and J. Hefner, "Guided lock acquisition in a suspended Fabry–Perot cavity," Opt. Lett. **20**, 2463–2465 (1995).
8. K. Kawabe, N. Mio, and K. Tsubono, "Automatic alignment-control system for a suspended Fabry–Perot cavity," Appl. Opt. **33**, 5498–5505 (1994).
9. E. Morrison, B. J. Meers, D. I. Robertson, and H. Ward, "Automatic alignment of optical interferometers," Appl. Opt. **33**, 5041–5049 (1994).
10. E. Morrison, B. J. Meers, D. I. Robertson, and H. Ward, "Experimental demonstration of an automatic alignment system for optical interferometers," Appl. Opt. **33**, 5037–5040 (1994).
11. R. W. P. Drever, J. L. Hall, F. V. Kowalski, J. Hough, G. M. Ford, A. J. Munley, and H. Ward, "Laser phase and frequency stabilization using an optical resonator," Appl. Phys. B: Photophys. Laser Chem. **31**, 97–105 (1983).
12. E. Hecht, *Optics* (Addison-Wesley, Reading, Mass., 1987), p. 368. We extend the term "Fabry–Perot" to include cavities with curved as well as flat mirrors in this paper.
13. A. E. Siegman, *Lasers* (University Science, Mill Valley, Calif., 1986), pp. 413–426.
14. M. Born and E. Wolf, *Principles of Optics* (Pergamon, Oxford, 1980), pp. 327–328.
15. A. E. Siegman, *Lasers* (University Science, Mill Valley, Calif., 1986), p. 437.
16. A. Yariv, *Optical Electronics* (Holt, Rinehart & Winston, New York, N.Y., 1985), pp. 294–296.
17. N. Uehara and K. Ueda, "Frequency stabilization of two diode-pumped Nd:YAG lasers locked to two Fabry–Perot cavities," Jpn. J. Appl. Phys. **33**, 1628–1633 (1994).
18. T. Day, E. K. Gustafson, and R. L. Byer, "Active frequency stabilization of a 1.062-μm, Nd:GGG, diode-laser-pumped nonplanar ring oscillator to less than 3 Hz of relative linewidth," Opt. Lett. **15**, 221–223 (1990).